Title

Autoinhibitory mechanism controls binding of centrosomin motif 1 to γ-tubulin ring complex.

Journal

Journal of Cell Biology, 222(7)

Authors

Yang, Shaozhong

Au, Franco

Li, Gefei

et al.

Publication Date

2023-07-03

DOI

10.1083/jcb.202007101

Peer reviewed

JCB Journal of Cell Biology

ARTICLE

Autoinhibitory mechanism controls binding of centrosomin motif 1 to γ-tubulin ring complex

Shaozhong Yang[1], Franco K.C. Au[1], Gefei Li[1], Jianwei Lin[2], Xiang David Li[2], and Robert Z. Qi[1,3]

The γ-tubulin ring complex (γTuRC) is the principal nucleator of cellular microtubules, and the microtubule-nucleating activity of the complex is stimulated by binding to the γTuRC-mediated nucleation activator (γTuNA) motif. The γTuNA is part of the centrosomin motif 1 (CM1), which is widely found in γTuRC stimulators, including CDK5RAP2. Here, we show that a conserved segment within CM1 binds to the γTuNA and blocks its association with γTuRCs; therefore, we refer to this segment as the γTuNA inhibitor (γTuNA-In). Mutational disruption of the interaction between the γTuNA and the γTuNA-In results in a loss of autoinhibition, which consequently augments microtubule nucleation on centrosomes and the Golgi complex, the two major microtubule-organizing centers. This also causes centrosome repositioning, leads to defects in Golgi assembly and organization, and affects cell polarization. Remarkably, phosphorylation of the γTuNA-In, probably by Nek2, counteracts the autoinhibition by disrupting the γTuNA–γTuNA-In interaction. Together, our data reveal an on-site mechanism for controlling γTuNA function.

Introduction

Most microtubule-organizing centers, including centrosomes and the Golgi complex, require γ-tubulin ring complexes (γTuRCs) to initiate microtubule growth and to organize microtubules into ordered arrays (Lüders and Stearns, 2007; Petry and Vale, 2015; Wu and Akhmanova, 2017). γTuRCs are assembled as a macromolecular structure whose core components are γ-tubulin and five other γ-complex proteins (GCPs), GCP 2–6 (Kollman et al., 2011). In each γTuRC, several γ-tubulin small complexes, which are a tetrameric assembly of two γ-tubulins, GCP2 and GCP3, are arranged with additional γ-tubulins and GCP 4–6 to form an asymmetric, microtubule-incompatible structure (Kollman et al., 2008; Liu et al., 2020; Wieczorek et al., 2020a; Wieczorek et al., 2020b; Consolati et al., 2020). Recently, it was proposed that the binding of α/β-tubulin heterodimers to the γ-tubulins may facilitate the transformation of the asymmetric structure into a symmetric, microtubule-compatible geometry (Thawani et al., 2020).

The microtubule-nucleating activity of γTuRCs is tightly controlled in a spatiotemporal manner. For instance, most γTuRCs are found in the cytosol where they exhibit little or no microtubule-nucleating activity (Moudjou et al., 1996; Bauer et al., 2016). However, it remains unclear how this nucleating activity is regulated. In human cells, CDK5RAP2 (also known as Cep215), a protein that localizes to both centrosomes and the Golgi, contains a short sequence that specifically interacts with γTuRCs and stimulates their microtubule-nucleating activity (Fong et al., 2008; Wang et al., 2010; Choi et al., 2010). This sequence, called the γTuRC-mediated nucleation activator (γTuNA), consists of ∼30 residues and is located within the first half of a sequence motif known as the centrosomin motif 1 (CM1; Sawin et al., 2004; Zhang and Megraw, 2007; Choi et al., 2010). To date, all γ-tubulin complex (γTuC)-recruiting proteins in organisms ranging from yeast to humans have been found to contain, as the γTuC-binding element, either CM1 alone or CM1 in combination with a second motif called the Spc110/Pcp1 motif (SPM; Lin et al., 2014). Furthermore, in addition to the canonical γTuNA, a bipartite γTuNA has recently been identified in TPX2, a critical factor that, in association with the protein complex augmin, induces γTuRC-dependent nucleation of branched microtubules (Alfaro-Aco et al., 2017).

Although the γTuNA motif is a significant element that binds to and stimulates γTuRCs in both yeast and human cells, the

[1]Division of Life Science and State Key Laboratory of Molecular Neuroscience, The Hong Kong University of Science and Technology, Hong Kong, China; [2]Department of Chemistry, The University of Hong Kong, Hong Kong, China; [3]Bioscience and Biomedical Engineering Thrust, The Hong Kong University of Science and Technology (Guangzhou), Guangzhou, China.

Correspondence to Robert Z. Qi: qirz@ust.hk

S. Yang's current affiliation is Department of Neurobiology, Affiliated Mental Health Center and Hangzhou Seventh People's Hospital, Zhejiang University School of Medicine, Hangzhou, Zhejiang, China. F.K.C. Au's current affiliation is Department of Cellular and Molecular Medicine, University of California at San Diego, La Jolla, CA, USA.

mechanism that regulates its binding to γTuRCs remains unclear. In this report, we describe a previously unrecognized autoinhibitory mechanism within CM1 that controls γTuNA binding to γTuRCs. We found that this autoinhibition is relieved by phosphorylation of the autoinhibitory domain at Ser112. The physiological importance of this autoinhibition is significant because the loss of autoinhibition in CDK5RAP2 results in a significant increase in the growth of centrosome- and Golgi-derived microtubules, which affects centrosome positioning, the connection between centrosomes and the Golgi, and causes defects in Golgi assembly and cell polarization. We have also identified the centrosomal kinase NIMA-related kinase 2 (Nek2) as a candidate kinase that phosphorylates CDK5RAP2 at Ser112 to relieve autoinhibition.

Results

CM1 contains a conserved autoinhibitory element

Alignment of CM1 sequences from CDK5RAP2 and its orthologs in lower eukaryotes revealed that CM1 consists of two conserved segments (aa 59–88 and 96–114 of CDK5RAP2) separated by a short linker sequence (Fig. 1 A). While the first conserved segment (59–88) is recognized as the γTuNA, the function of the second conserved segment (96–114) has remained unclear. To investigate the function of the second conserved segment, we constructed two CDK5RAP2 fragments, 1–100 and 1–126, containing the γTuNA alone and the entire CM1, respectively, and compared their γTuRC-binding activity by performing transient-expression and immunoprecipitation assays. We found that the γTuNA-only construct (1–100) robustly coprecipitated γ-tubulin, but this coprecipitation activity was diminished by >90% in the entire CM1 (1–126; Fig. 1 B). Similar results were obtained when we compared the γTuRC-binding activity of the fragments 51–100 and 51–150, both of which lack the amino-terminal region upstream of the γTuNA (Fig. 1 C). These results indicate that extending the γTuNA to include the second conserved segment (96–114) strongly inhibits γTuRC-binding activity.

To further investigate the effect of the second conserved segment, we performed a mutational analysis. First, we individually mutated three conserved residues within this region and tested the mutants for their γTuRC-binding activity in coimmunoprecipitation experiments. The mutation K101A did not cause any change in γTuRC-binding activity (Fig. 1 D), whereas I104A drastically increased the binding activity and E105A moderately increased the activity (Fig. 1 D). We then created and tested the double mutant I104A/E105A, which exhibited further enhanced activity compared with the single mutant I104A (Fig. 1 E). Moreover, we engineered the double mutation I104A/E105A into full-length CDK5RAP2 and found that the mutation increased the γTuRC-binding activity of CDK5RAP2 by ∼12-fold (Fig. 1 F). In agreement with the binding results, the entire CM1 construct showed a much lower activity of γTuRC stimulation than the γTuNA protein (Fig. S1). Collectively, these results support the conclusion that the second conserved region harbors inhibitory activity toward the γTuNA. Therefore, we hereafter refer to the second conserved region as the γTuNA-inhibitor (γTuNA-In).

To understand the mechanism of autoinhibition, the interaction between the γTuNA and γTuNA-In domains was further studied. Co-expression of the γTuNA construct (FLAG-1–100) with the γTuNA-In construct (GFP-90–126) or the γTuNA-In mutant I104A/E105A was performed to validate the interaction. The immunoprecipitation of the γTuNA robustly coprecipitated the γTuNA-In but failed to coprecipitate the I104A/E105A mutant or GFP alone (Fig. 2 A). In direct-binding assays, the γTuNA-In recombinant protein readily bound to the γTuNA (Fig. 2 B). In a previous study, it was shown that within the γTuNA, Phe75 is crucial for γTuRC binding, and the F75A mutation abolished the binding activity (Choi et al., 2010). Therefore, the F75A mutant of the γTuNA was tested, and its binding activity toward γTuNA-In was significantly reduced (Fig. 2 C). Together, these results reveal the critical involvement of Ile104–Glu105 and Phe75 in the interaction between the γTuNA and γTuNA-In domains.

CM1 autoinhibition participates in control of centrosome- and Golgi-based nucleation

We established stable hTERT RPE-1 (RPE-1) sublines with inducible expression of CDK5RAP2. In these cells, epitope-tagged CDK5RAP2 and its I104A/E105A mutant were expressed at minimal levels in the absence of doxycycline, and upon induction, the proteins were expressed at levels similar and close to those of the endogenous protein (Fig. 3 A). Furthermore, we used siRNA-mediated knockdown to effectively suppress the expression of endogenous CDK5RAP2 in these cells by over 90% (Fig. 3 A). The I104A/E105A-expressing cells did not exhibit any overt defects in cell proliferation.

Quantitative analysis of microtubule regrowth after cold-induced microtubule depolymerization revealed that, relative to wild-type CDK5RAP2-expressing cells, I104A/E105A-expressing cells showed significant increases in centrosome-based and Golgi-based regrowth (∼2.2- and ∼5.4-fold, respectively; Fig. 3 B). Microtubule nucleation was also slightly increased in the cytosol in I104A/E105A-expressing cells. We also evaluated microtubule regrowth after nocodazole-induced depolymerization. After nocodazole washout, microtubules regrew from Golgi ministacks throughout the cytoplasm and from centrosomes (Fig. S2). After a short regrowth, we could unequivocally identify microtubules nucleated on the Golgi ministacks and those nucleated on the centrosomes (Fig. S2), and the results corroborate those of the assay after cold-induced depolymerization. Furthermore, in the I104A/E105A-expressing cells, the intensity of γ-tubulin on centrosomes was moderately (∼20%) higher than that in wild-type CDK5RAP2-expressing cells, although the Golgi intensity of γ-tubulin did not differ significantly (Fig. 3 C). Together, our results indicate that CDK5RAP2-CM1 autoinhibition exerts a strong control on γTuRC stimulation on centrosomes and the Golgi complex.

Loss of CDK5RAP2-CM1 autoinhibition affects centrosome positioning and association with Golgi

In our assays of cells expressing wild-type and I104A/E105A mutant CDK5RAP2 (Fig. 3, B and C), we observed that expression of the I104A/E105A mutant increased the proportion of cells in

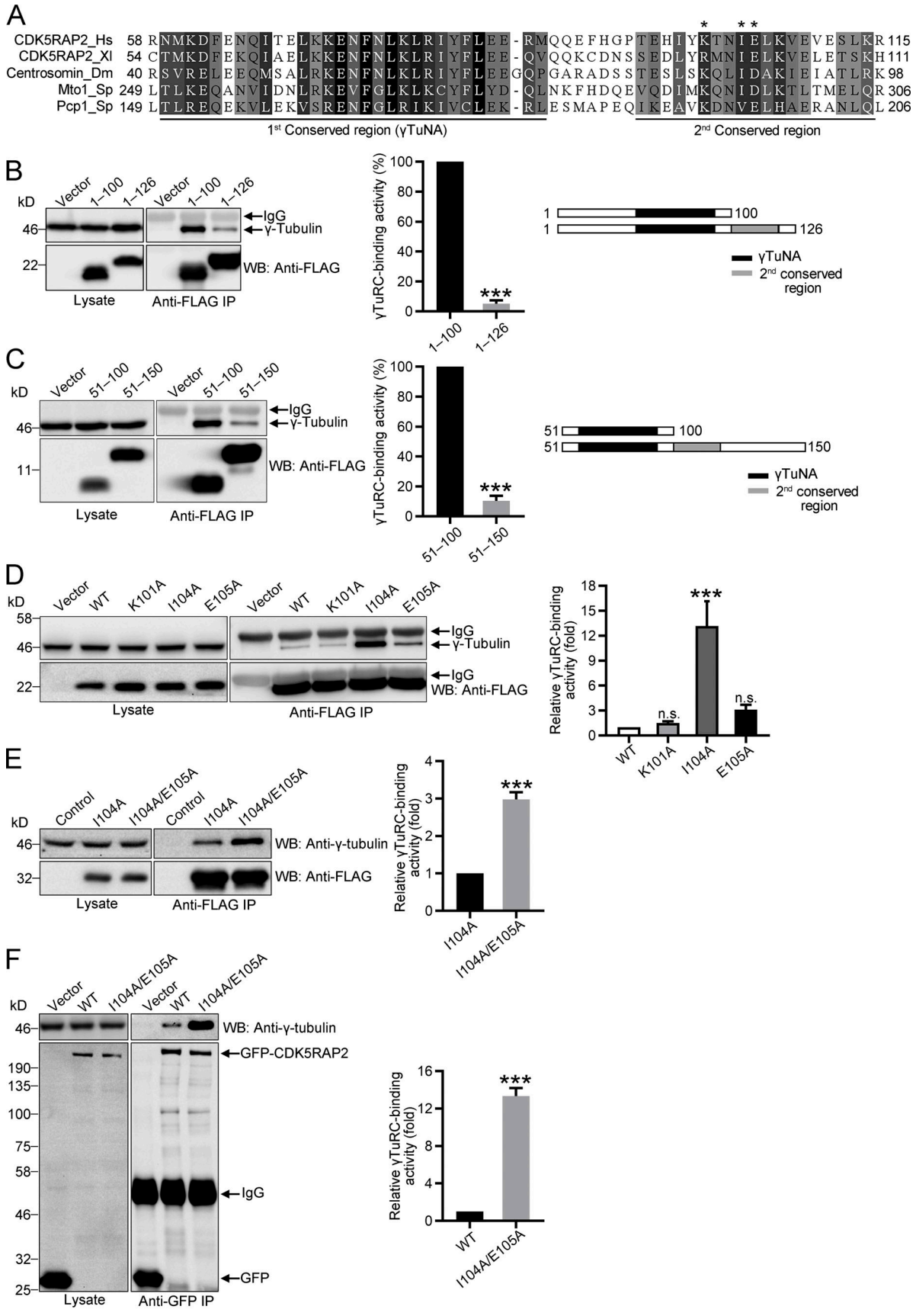

Figure 1. **The second conserved element in CM1 inhibits γTuNA binding to γTuRCs. (A)** Sequence alignment of CM1 from CDK5RAP2 and its orthologs. Hs, *Homo sapiens*; Xl, *Xenopus laevis*; Dm, *Drosophila melanogaster*; and Sp, *Schizosaccharomyces pombe*. Asterisks: sites mutated in constructs shown in D. **(B and C)**

CDK5RAP2 fragments (FLAG-tagged) were transiently expressed in HEK293T cells for anti-FLAG immunoprecipitation (IP). Immunoprecipitates and cell-lysate inputs were immunoblotted (WB) with indicated antibodies (n = 4 for 1–100 and 1–126; n = 3 for 51–100 and 51–150). Presented are γTuRC-binding activities relative to that of the wild-type construct (WT). **(D)** CDK5RAP2 fragment 1–140 and its mutants were ectopically expressed and immunoprecipitated as in B and C (n = 5, 3, 5, and 3 for WT, K101A, I104A, and E105A, respectively). WT, wild-type 1–140. **(E)** Purified recombinant proteins of CDK5RAP2(1–140) mutants (FLAG-tagged) were incubated with HEK293T cell lysates and then subjected to anti-FLAG immunoprecipitation (n = 3 per group). **(F)** GFP-tagged full-length CDK5RAP2 (WT) and I104A/E105A mutants were transiently transfected into HEK293T cells for anti-GFP immunoprecipitation (n = 4 per group). **(B–F)** Lysate or protein inputs (4%) and immunoprecipitates (50%) were analyzed on immunoblots, and data are presented as means ± SEM from at least three independent experiments. Unpaired t test used in B, C, E, and F, and one-way ANOVA used in D; ***, P < 0.001; n.s., not significant, P ≥ 0.05.

which centrosomes appeared either above or below the nuclei; in most of these cells, the centrosomes were situated below the nuclei (Fig. S3). Therefore, we analyzed the effects of transgene expression on the subcellular position of centrosomes. We measured the distances between the centrosomes and the cell centroid and adopted a published method of expressing the distances relative to the effective cell radius to minimize the influence of cell size and shape variations (Hale et al., 2011). Compared to cells expressing wild-type CDK5RAP2, cells expressing the I104A/E105A mutant showed a significant reduction in the distance between centrosomes and the cell centroid (28.9 versus 20.7% of the effective radius in cells expressing wild-type and I104A/E105A CDK5RAP2, respectively; Fig. 4, A and B). Conversely, centrosomes were within 20% of the effective cell radius from the cell centroid in ∼37.0% of the cells expressing the wild-type protein versus ∼56.4% of the cells expressing the I104A/E105A mutant (Fig. 4, A and B).

To assess whether Golgi-derived microtubules participate in centrosome centralization, we treated cells with brefeldin A (BFA) to disassemble Golgi complexes. We found that Golgi disassembly did not affect centrosome centralization induced by the I104A/E105A mutant (Fig. 4, A and B). Collectively, our results indicate that in cells expressing the I104A/E105A mutant, the overgrowth of centrosome-derived microtubules causes centrosome relocation toward the cell center and that Golgi-derived microtubules are dispensable for this centralization process.

Re-expression of the I104A/E105A mutant in RPE-1 cells resulted in the dissociation of the Golgi complex and centrosomes, as evidenced by an increase in the average distance between them from 1.53 µm in cells expressing wild-type CDK5RAP2 to 2.83 µm in cells expressing the I104A/E105A mutant, and the proportion of cells expressing the mutant protein with an increased centrosome–Golgi distance (distance larger than the average distance in cells expressing wild-type protein) was also significantly higher (Fig. 4, A and C). These findings suggest that the activity of centrosome-based microtubule growth is a crucial determinant of the relative positions of the Golgi and centrosomes, given that the Golgi organizes an asymmetric microtubule array that radiates from the cis- to trans-networks (Efimov et al., 2007).

Loss of CDK5RAP2-CM1 autoinhibition impairs Golgi assembly and cell polarization

During Golgi assembly, Golgi-derived and centrosome-derived microtubules facilitate, respectively, the fusion of Golgi mini-stacks dispersed in the cytoplasm (referred to as the G stage) and the translocation of the fused stacks toward the centrosome

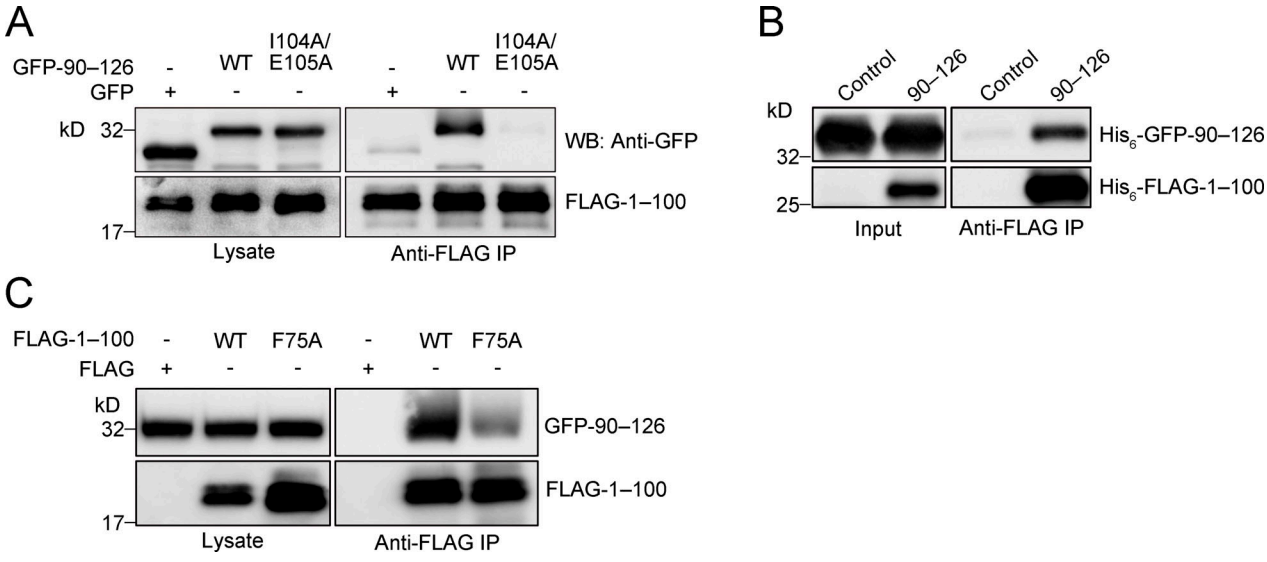

Figure 2. **γTuNA-In binds directly to γTuNA. (A)** CDK5RAP2 1–100 (FLAG-tagged) was transiently coexpressed with 90–126 (GFP-tagged) wild-type (WT) or I104A/E105A in HEK293T cells, and anti-FLAG immunoprecipitates were immunoblotted (WB). **(B)** Binding assay of recombinant proteins CDK5RAP2 1–100 and 90–126. Anti-FLAG immunoprecipitation was followed by anti-GFP and anti-FLAG immunoblotting. **(C)** FLAG-tagged 1–100 or F75A mutant was transiently co-expressed with GFP-tagged 90–126 in HEK293T cells for anti-FLAG immunoprecipitation. **(A–C)** Lysate or protein inputs (4%) and immunoprecipitates (50%) were analyzed on immunoblots.

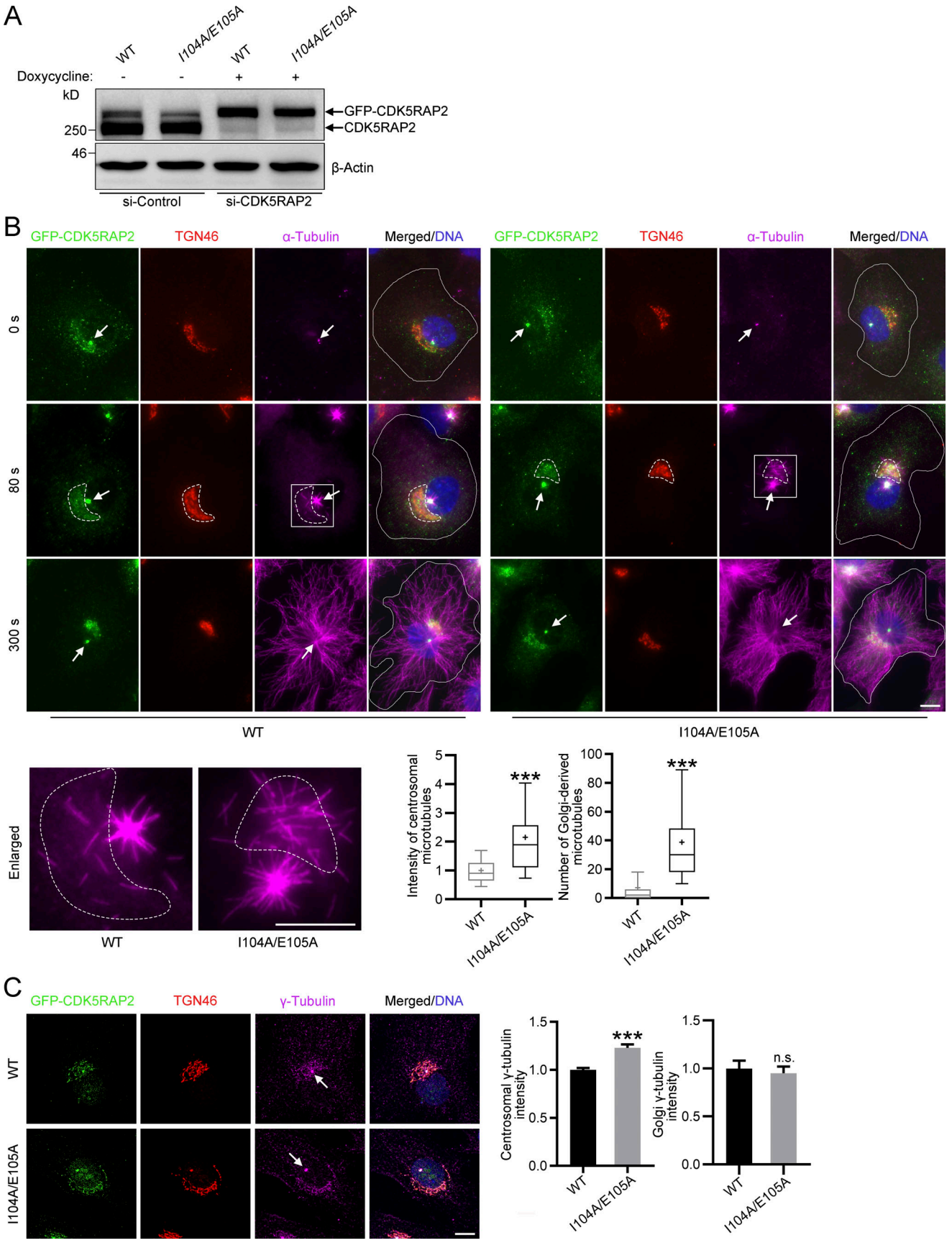

Figure 3. **Microtubule regrowth on centrosomes and Golgi of cells expressing CM1 autoinhibition-defective mutant of CDK5RAP2. (A)** Immunoblots of extracts from RPE-1 cells with doxycycline-inducible expression of GFP-CDK5RAP2 wild-type (WT) or I104A/E105A mutant. Cells were also transfected with

cdk5rap2-targeting or control siRNA. **(B and C)** Assays were performed on RPE-1 cells expressing GFP-CDK5RAP2 WT or I104A/E105A and depleted of endogenous CDK5RAP2 (through RNAi). **(B)** Microtubule regrowth assayed after cold-induced depolymerization. Immunostaining was performed with indicated antibodies (n = 62 and 63 for centrosomal microtubule regrowth in WT- and I104A/E105A-expressing cells, respectively; n = 125 and 122 for Golgi-derived microtubule regrowth in WT- and I104A/E105A-expressing cells, respectively). Arrows: centrosomes; white lines: cell boundaries; dash lines: Golgi boundaries. Boxed areas are enlarged. Box and whisker plot: lower and upper edges, 25th and 75th percentiles; lower and upper whiskers, 10th and 90th percentiles; lines within boxes, medians; "+" within boxes, averages. **(C)** Immunostaining with indicated antibodies (n = 139 and 143 for centrosomal γ-tubulin in WT- and I104A/E105A-expressing cells, respectively; n = 103 and 104 for Golgi γ-tubulin in WT- and I104A/E105A-expressing cells, respectively). **(B and C)** Nuclei were stained with Hoechst 33258. Data are presented as means ± SEM from at least three independent experiments. Unpaired t test used in B and C; ***, P < 0.001; n.s., not significant, P ≥ 0.05. Scale bars, 10 µm.

(referred to as the C stage; Miller et al., 2009). We disassembled Golgi complexes in RPE-1 cells re-expressing wild-type and I104A/E105A CDK5RAP2 by treating the cells with nocodazole, and after washing out the nocodazole, we monitored the reassembly process. In cells expressing the wild-type protein, both G-stage and C-stage assemblies occurred after nocodazole washout, and an intact Golgi was formed 1 h after washout (Fig. 5 A). By contrast, in I104A/E105A-expressing cells, although Golgi ministacks were clustered in the cytoplasm, as in cells expressing the wild-type protein, a considerable slowing was measured in both the translocation of Golgi patches toward centrosomes and the formation of the Golgi near centrosomes (Fig. 5 A). Therefore, the loss of CM1 autoinhibition impaired Golgi assembly at the C-stage but not at the G-stage.

During cell polarization, both the Golgi and the centrosomes are reoriented toward the leading edge; this process involves Golgi-derived microtubules and Golgi-centrosome association (Miller et al., 2009; Rivero et al., 2009; Yadav et al., 2009; Hurtado et al., 2011). We induced cell polarization through scratch wounding on monolayer cultures of the aforementioned RPE-1 sublines rescued with wild-type and I104A/E105A CDK5RAP2, and we examined the reorientation of the Golgi and centrosomes. In cells rescued with the I104A/E105A mutant, reorientation of both centrosomes and Golgi complexes was markedly slower than that in cells rescued with the wild-type protein (Fig. 5 B). This result was quantified by measuring, at several time points post-wounding, the angles required for reorienting the centrosomes and Golgi complexes to face straight toward the wound edge (Fig. 5 B). The time-course analysis revealed that cells expressing the I104A/E105A mutant showed delayed reorientation of both centrosomes and Golgi complexes; at 7 h post-wounding, the angles for centrosomes and Golgi complexes were ∼67.3° and ∼53.1°, respectively, whereas, in cells expressing the wild-type protein, the angles were ∼31.8° and ∼30.4° for centrosomes and Golgi complexes, respectively (Fig. 5 B). Thus, the loss of CM1 autoinhibition interferes with the reorientation of both centrosomes and the Golgi complex.

CM1 phosphorylation disrupts γTuNA–γTuNA-In interaction to antagonize autoinhibition

Nek2A has been reported to cause phosphorylation of CDK5RAP2 (Cervenka et al., 2016). Among the sites of Nek2A-induced phosphorylation, Thr102 and Ser112 are located within the γTuNA-In region (Fig. 1 A). While Ser112 is conserved or conservatively substituted in the metazoan orthologs of CDK5RAP2, Thr102 is not conserved. Moreover, phosphorylation at Thr102 was reported not to affect the γTuRC-binding activity of CM1 (Hanafusa et al., 2015). Thus, we investigated the function of Ser112 phosphorylation by substituting the residue with Asp to create a phosphomimetic mutant (S112D) and with Ala to create a non-phosphorylatable mutant (S112A). In pulldown assays, wild-type CDK5RAP2 and the S112A mutant exhibited similar γTuRC-binding activity, whereas the S112D mutant exhibited significantly higher binding activity (Fig. 6 A). Furthermore, the phosphomimetic mutation increased the activity to a similar level as the I104A/E105A mutation (Fig. 1 F and Fig. 6 A). Next, we tested the effect of S112D on γTuNA-In binding to the γTuNA. In contrast to wild-type γTuNA-In, the S112D mutant showed drastically diminished binding activity toward the γTuNA (Fig. 6 B), which agrees with the augmented binding of γTuRCs by CM1(S112D). These results strongly suggest that Ser112 phosphorylation disrupts the interaction between the γTuNA-In and the γTuNA to counteract CM1 autoinhibition.

To characterize the physiological effects of Ser112 phosphorylation, we created stable RPE-1 sublines inducibly expressing CDK5RAP2(S112D) and used these sublines, along with wild-type CDK5RAP2 sublines, in several assays. Prior to the assays, we depleted endogenous CDK5RAP2 by siRNA transfection and induced expression of wild-type CDK5RAP2 and the S112D mutant to levels similar to endogenous CDK5RAP2 in parent cells (Fig. 6 C). First, we measured microtubule regrowth after cold-induced depolymerization and found that S112D-expressing cells showed significantly higher regrowth activities on both centrosomes and Golgi complexes than wild-type-expressing cells (∼1.9- and ∼3.0-fold, respectively; Fig. 6 D). These results are consistent with those obtained from the rescue by the I104A/E105A mutant (Fig. 3 B), indicating that S112D and I104A/E105A have similar effects in disrupting autoinhibition. We then examined the effects of S112D on centrosome positioning, Golgi reassembly, and centrosome and Golgi reorientation. Similar to I104A/E105A, the S112D mutation reduced the distance between centrosomes and the cell centroid (Fig. S4), impaired Golgi reassembly after nocodazole washout (Fig. S5 A), and interfered with the scratch-wounding-induced reorientation of centrosomes and Golgi complexes (Fig. S5 B).

To confirm the phosphorylation of Ser112 by Nek2A, we first examined the interaction between Nek2A and CDK5RAP2. We detected robust binding of Nek2A and CDK5RAP2 in a coimmunoprecipitation assay (Fig. 7 A). After the phosphorylation reaction, proteins were resolved by SDS-PAGE, and the bands corresponding to the CM1 protein CDK5RAP2 1–140 were tryptically digested and analyzed by mass spectrometry. Phosphorylation of Ser112 was readily found in the Nek2A-treated sample

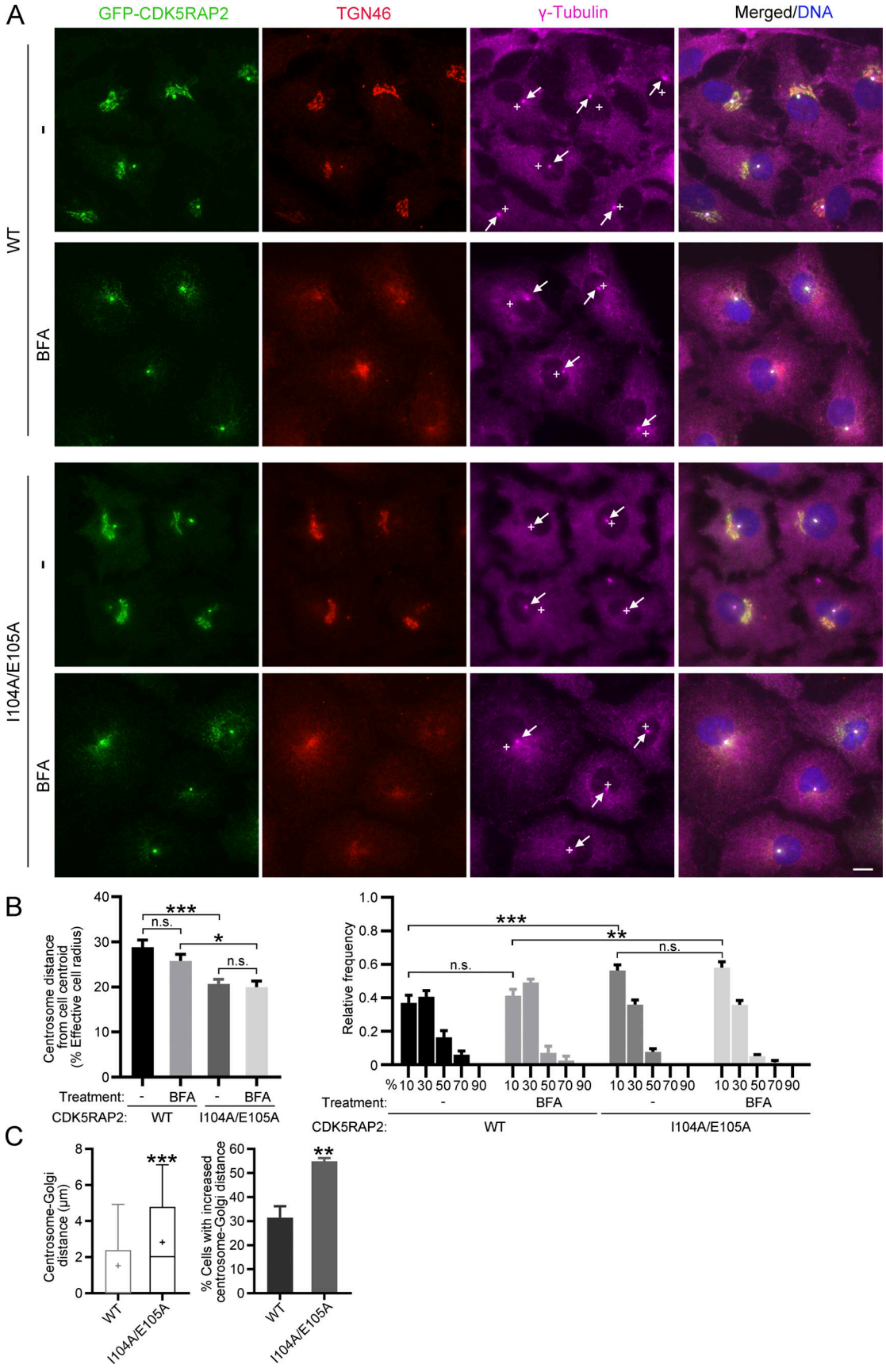

Figure 4. **Interfering with CDK5RAP2-CM1 autoinhibition affects centrosome positioning and its association with the Golgi. (A–C)** RPE-1 sublines with inducible expression of GFP-tagged CDK5RAP2 wild-type (WT) or I104A/E105A mutant were depleted of endogenous CDK5RAP2 (through RNAi). Cells were

treated with or without BFA. **(A)** Representative micrographs showing cell staining. Nuclei were stained with Hoechst 33258. "+", cell centroid; arrows: centrosomes. Scale bar, 10 µm. **(B)** Measured distances between centrosomes and cell centroids are presented as values relative to effective cell radius (left) or as frequency distributions (right). Circularized effective cell area was divided into five regions of equal radius; first bin (10%): cells harboring centrosomes within 20% of effective radius from cell centroid (n = 112 and 117 for WT- and I104A/E105A-expressing cells, respectively; in the BFA-treated group, n = 87 and 86 for WT- and I104A/E105A-expressing cells, respectively). **(C)** Distance between centrosomes and Golgi (n = 422 and 396 for WT and I104A/E105A, respectively). Box and whisker plot: "+" within boxes, averages. **(B and C)** Data are presented as means ± SEM from at least three independent experiments. One-way ANOVA was used in B (left), two-way ANOVA was used in B (right), and unpaired t test was used in C. ***, P < 0.001; **, P < 0.01; *, P < 0.05; n.s., not significant, P ≥ 0.05.

(Fig. 7 B), but it was not detected in the sample treated in the absence of Nek2A. Therefore, Nek2A catalyzed Ser112 phosphorylation. To further assess the involvement of Nek2 in the regulation of cellular microtubule nucleation, we performed a microtubule regrowth assay on cells transfected with control or *nek2*-targeting siRNA; the transfection of the *nek2*-targeting siRNA effectively suppressed Nek2 expression (Fig. 7 C). The knockdown of Nek2 significantly reduced centrosome-based regrowth but did not show any obvious effect on Golgi-based regrowth (Fig. 7 D). These results revealed that Nek2 is involved in microtubule nucleation on centrosomes but is dispensable for Golgi-based nucleation.

Discussion

We have revealed here that within CM1 a conserved segment located adjacent to the γTuNA serves as an autoinhibitory element and we have named this segment the γTuNA-In. This CM1 autoinhibition is highly potent: it blocked >90% of the γTuRC-binding activity of the γTuNA. Therefore, the γTuNA-In exerts a stringent on-site control of the γTuNA function. Mechanistically, we found that the γTuNA-In binds to the γTuNA and, furthermore, the binding requires Phe75, a γTuNA residue that is critically involved in the interaction between the γTuNA and γTuRCs (Choi et al., 2010). Notably, the I104A/E105A mutation within the γTuNA-In abolished the γTuNA-In binding to and inhibition of the γTuNA, thus providing control for establishing the autoinhibitory effect. Our findings suggest that CM1 is folded into a closed form in which the γTuNA-In blocks the γTuRC-binding site on the γTuNA. Recently, it was shown that the γTuNA exists as a dimer and, further, dimerization is required for binding to and activation of γTuRCs (Rale et al., 2022; Wieczorek et al., 2020a). It is also possible that the γTuNA-In inhibits the γTuNA activity toward γTuRCs by disrupting γTuNA dimerization.

We found that the loss of CM1 autoinhibition in CDK5RAP2 significantly enhanced microtubule nucleation on centrosomes and the Golgi, but only caused a moderate increase or no change in γ-tubulin levels on centrosomes and the Golgi, respectively (Fig. 3). These data suggest that in mammalian cells, CDK5RAP2 plays a significant role in stimulating rather than attaching γTuRCs to centrosomes and the Golgi. Several γTuRC-binding proteins are known to be involved in recruiting γTuRCs to centrosomes and the Golgi, including Nedd1 (also known as GCP-WD), pericentrin, AKAP450, and myomegalin variant 8, in addition to CDK5RAP2 (Lüders et al., 2006; Haren et al., 2006; Fong et al., 2008; Wang et al., 2014; Lin et al., 2014). Nedd1 was reported to tether γTuRCs to centrosomes and spindle microtubules, while AKAP450, in association with myomegalin variant 8, plays a key role in γTuRC attachment to the Golgi (Lüders et al., 2006; Haren et al., 2006; Rivero et al., 2009; Wang et al., 2014). Our data suggest that upon the removal of CM1 autoinhibition, CDK5RAP2 primarily binds to and stimulates γTuRCs present on centrosomes or the Golgi. Therefore, CDK5RAP2 binds to γTuRCs in a tightly controlled manner on centrosomes and the Golgi.

In interphase cells, centrosomes are typically located near but not at the cell centroid. Loss of CDK5RAP2-CM1 autoinhibition repositioned centrosomes toward the cell center and dissociated them from the Golgi (Fig. 4). Centrosome positioning results from the balancing of forces associated with centrosome-derived microtubules and weaker, myosin-generated forces (Burakov et al., 2003). Specifically, growing microtubules pushing against the cell cortex generate forces that drive the centrosome toward the cell center; conversely, antagonistic pulling forces generated on microtubules by cortical dynein direct the centrosome toward the cell periphery. The loss of CDK5RAP2-CM1 autoinhibition enhanced microtubule nucleation on centrosomes (Fig. 3) and thereby increased the number of centrosome-derived microtubules. Furthermore, computational simulations have indicated that an increase in microtubule numbers from centrosomes increases the net pushing forces, which would direct centrosomes toward the cell center (Zhu et al., 2010; Letort et al., 2016). Notably, because of centrosome repositioning toward the cell center, the centrosomes were detached from the Golgi in cells expressing the CM1 autoinhibition-defective mutant of CDK5RAP2 (Fig. 4). This detachment supports the existence of centrosome-independent mechanisms underlying Golgi positioning, and such mechanisms have been implicated in several studies (Magdalena et al., 2003; Taverna et al., 2016).

Golgi-derived microtubules act together with centrosome-derived microtubules in several Golgi functions, such as Golgi assembly, structural organization, and reorientation (Rivero et al., 2009; Miller et al., 2009). By using the CM1 autoinhibition-deficient mutant of CDK5RAP2 (i.e., the I104A/E105A mutant), we found that the aberrantly increased growth of Golgi-derived microtubules impaired not only Golgi reassembly after nocodazole-induced disassembly but also Golgi reorientation. These phenotypes resemble those observed following the knockdown of the DNA polymerase δ catalytic subunit, a γTuRC inhibitor that resides on the Golgi complex (Shen et al., 2017). It was reported that centrosome dissociation from the Golgi also impairs Golgi reassembly after disassembly and interferes with the centrosome and Golgi reorientation during cell polarization (Hurtado et al., 2011). Therefore, the defects in

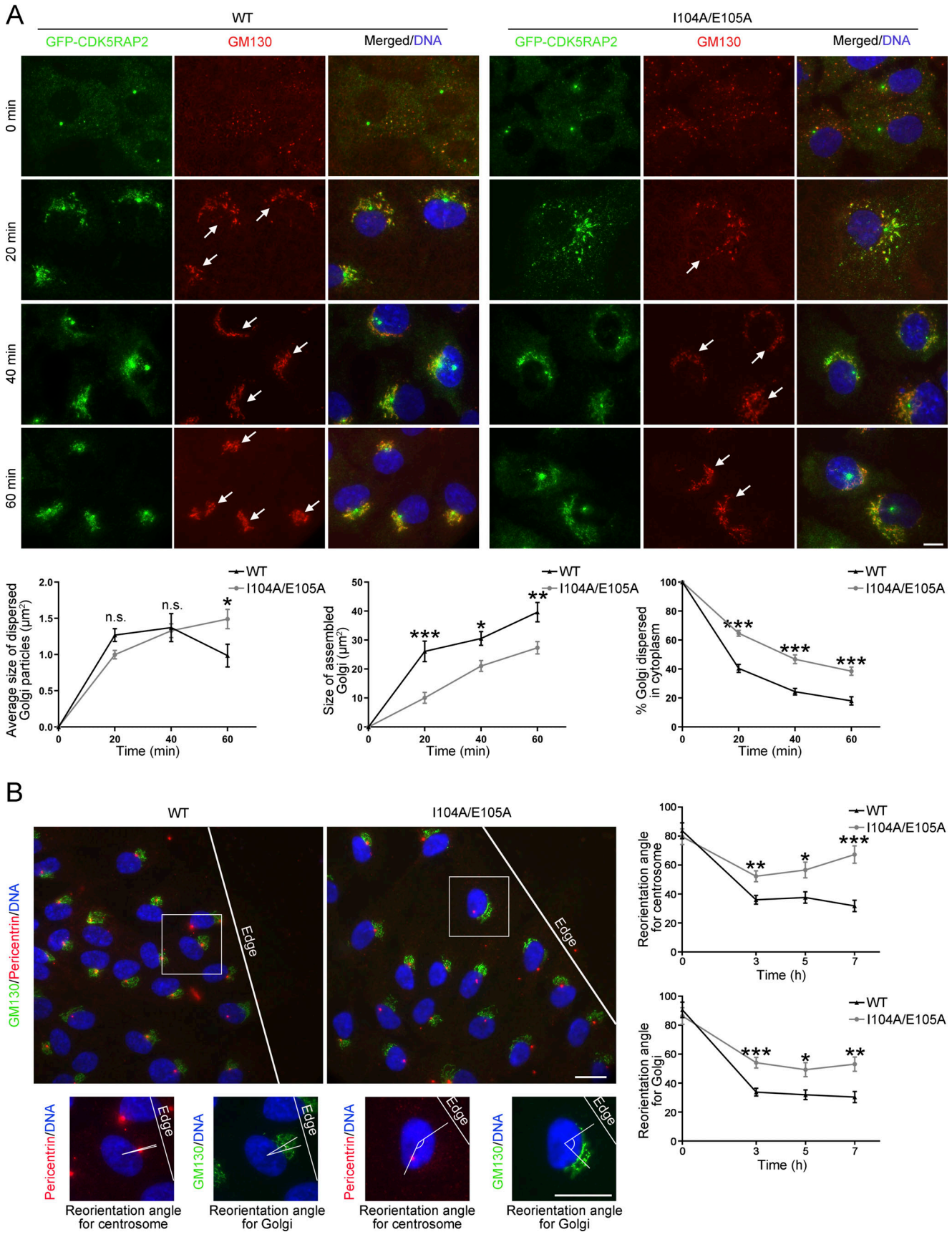

Figure 5. **Rescue by I104A/E105A expression affects Golgi reassembly and cell polarization. (A)** Golgi reassembly after nocodazole washout was tested on RPE-1 cells expressing wild-type (WT) or I104A/E105A GFP-CDK5RAP2 and depleted of endogenous CDK5RAP2. Cells were fixed at various time points for

immunofluorescence staining; nuclear DNA was stained with Hoechst 33258. *n* = 67, 79, and 60 for WT at 20, 40, and 60 min, respectively; *n* = 76, 67, and 71 for I104A/E105A at 20, 40, and 60 min, respectively. Quantification data show the average size of individual Golgi particles dispersed in the cytoplasm, the size of Golgi assembled near the centrosomes, and the proportion of Golgi dispersed in the cytoplasm. **(B)** Wounding-induced reorientation of centrosomes and Golgi was examined at various time points in RPE-1 cells. Cells were stained for GM130 and pericentrin, and reorientation angles for centrosomes and Golgi complexes were measured (*n* = 73, 118, 68, and 67 for WT at 0, 3, 5, and 7 h; *n* = 73, 125, 73, and 69 for I104A/E105A at 0, 3, 5, and 7 h, respectively). Box: magnified cell image for illustrating reorientation angles for centrosomes and Golgi. **(A and B)** Data are presented as means ± SEM from at least three independent experiments. Two-way ANOVA was used in A and B. ***, P < 0.001; **, P < 0.01; *, P < 0.05; n.s., not significant, P ≥ 0.05. Scale bars, 10 and 20 µm in A and B, respectively.

Golgi assembly and cell polarization observed in I104A/E105A- or S112D-expressing cells could result from both the aberrant growth of Golgi-derived microtubules and the dissociation of centrosomes from the Golgi.

Protein phosphorylation is a commonly seen mechanism that dissociates autoinhibitory domains from their targets, thus counteracting autoinhibition (Pufall and Graves, 2002). Nek2 induces CDK5RAP2 phosphorylation at Ser112, a residue located within the γTuNA-In, in cells (Cervenka et al., 2016) and catalyzes Ser112 phosphorylation in vitro (Fig. 7 B). The phosphomimetic mutation of Ser112 showed a similar effect as the mutation of Ile104-Glu105, a dipeptide within the γTuNA, to disrupt the interaction between the γTuNA and the γTuNA-In, which leads to an "open," active state of CM1. Therefore, Ser112 phosphorylation is sufficient to relieve autoinhibition. Nek2 is a centrosomal kinase that acts at the onset of mitosis to induce centrosome disjunction (Fry et al., 1998). We found that silencing Nek2 expression compromised centrosome-based microtubule nucleation but did not affect Golgi-based nucleation (Fig. 7 D). Our data suggest that Nek2 likely phosphorylates Ser112 on centrosomes. However, further studies are required to determine whether the phosphorylation of Ser112 is cell-cycle-regulated and whether Nek2 is involved in centrosome maturation by phosphorylating this residue.

Given that the γTuNA-In is conserved from human to yeast and Ser112 is conserved or conservatively substituted in metazoan CM1 sequences (Fig. 1 A), the autoinhibition characterized here for CM1 is a conserved mechanism and the phosphorylation-mediated removal of the autoinhibition is likely to be conserved in metazoans. It has been recently shown that in *Drosophila*, the centrosomal isoform of the centrosomin contains a region amino-terminal to CM1 that inhibits the γTuRC-binding activity of CM1 (Tovey et al., 2021). However, this sequence is not conserved in mammalian CDK5RAP2. Moreover, the corresponding region in human CDK5RAP2 does not inhibit the CM1 activity (Tovey et al., 2021; Fig. 1 B). Therefore, although CM1 possesses a conserved autoinhibitory element, there are unique features of CM1 regulation in different species.

Materials and methods

Plasmid constructs

CDK5RAP2 fragment constructs were generated from a CDK5RAP2 cDNA (Fong et al., 2008) by using standard molecular cloning techniques, and CDK5RAP2 mutants were created through Single-Primer Reactions IN Parallel site-directed mutagenesis (Edelheit et al., 2009). To prepare inducible RPE-1 sublines, GFP-CDK5RAP2 and its mutants were cloned together with a Kozak sequence into pRetroX-tight-pur (Clontech) by using the Gibson assembly method (Gibson Assembly Master Mix, New England Biolabs). The GFP nanobody plasmid was acquired from Dr. Kazuhisa Nakayama (Kyoto University, Kyoto, Japan; plasmid #61838; Addgene; Katoh et al., 2015).

Recombinant proteins and antibodies

His_6-tagged recombinant proteins were expressed in *Escherichia coli* BL21 (DE3), purified using Ni^{2+}-nitrilotriacetic acid resin (Qiagen), dialyzed against phosphate-buffered saline (137 mM NaCl, 2.7 mM KCl, 4.3 mM Na_2HPO_4, 1.47 mM KH_2PO_4, pH 7.4) supplemented with 10% glycerol, and stored in −80°C. Antibodies against CDK5RAP2 and GFP (both used at 1:500 dilution) have been described previously (Fong et al., 2008; Au et al., 2017). The following antibodies were purchased: anti-γ-tubulin (1:1,000, GTU88), anti-FLAG (1:1,000, rabbit polyclonal), anti-β-actin (1:5,000, AC-15), and anti-α-tubulin (1:600, DM1A), Sigma-Aldrich; anti-GM130 (1:600, monoclonal), BD Biosciences; anti-TGN46 (1:600, sheep polyclonal), Serotec; anti-pericentrin (1:300, C-16), Santa Cruz Biotechnology; and DyLight or Alexa Fluor secondary antibodies (1:600), Thermo Fisher Scientific.

Cell culture, transfection, and stable cell lines

All cell lines used here were purchased from American Type Culture Collection. HEK293T (CRL-11268) and Phoenix-AMPHO (CRL-3213) cells were cultured in Dulbecco's modified Eagle's medium (DMEM, Gibco) and RPE-1 (CRL-4000) cells were cultured in DMEM/Ham's F12 (1:1) medium; both media were supplemented with 10% fetal bovine serum and 1% penicillin/streptomycin. Cells were grown in a humidified environment containing 5% CO_2 at 37°C and were free of mycoplasma contamination. Stable RPE-1 sublines with Tet-on inducible CDK5RAP2 expression were generated using pRetroX-tight-pur and pRetroX-Tet-On Advanced (Clontech). Plasmids were transfected using polyethylenimine (Polysciences) into HEK293T and Phoenix-AMPHO cells and siRNAs were transfected using Lipofectamine RNAiMAX (Thermo Fisher Scientific). siRNAs targeting *cdk5rap2* (5′-UGGAAGAUCUCCUAACUAA-3′) were used as previously reported (Fong et al., 2008). To disrupt the Golgi, cells were treated with 5 µg/ml BFA in a culture medium for 2 h (Vinogradova et al., 2012).

Immunofluorescence microscopy and image analysis

RPE-1 cells grown on glass coverslips were fixed for 15 min with methanol at −20°C or 4% paraformaldehyde in PHEM buffer (60 mM PIPES-KOH, 25 mM HEPES, pH 6.9, 10 mM EGTA, 2 mM $MgCl_2$) containing 0.5% Triton X-100 at room temperature.

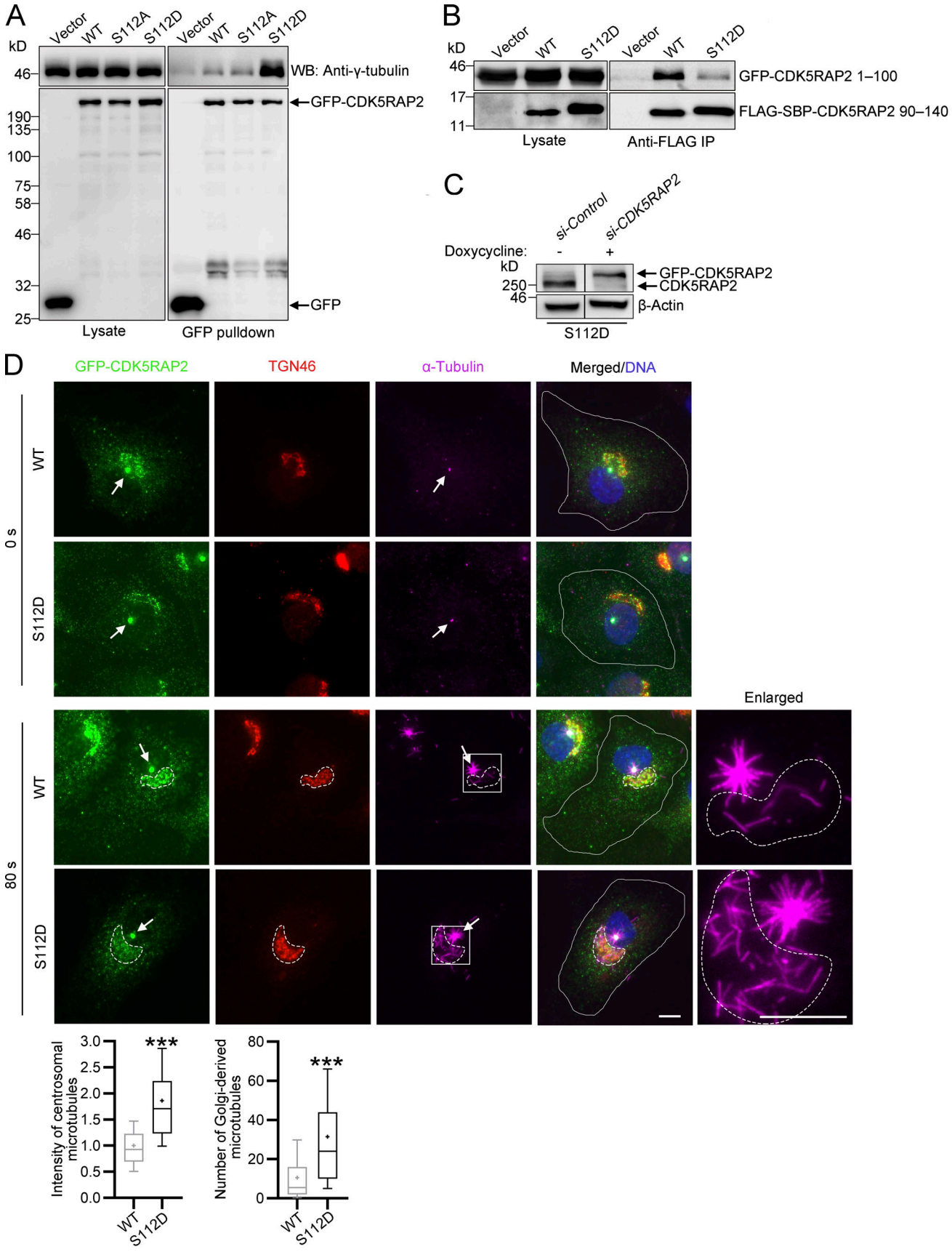

Figure 6. **Ser112 phosphorylation relieves CM1 autoinhibition. (A)** GFP-CDK5RAP2 (WT) and its mutants were transiently transfected into HEK293T cells for a pulldown using GFP nanobody-coupled beads. The pulldowns were examined by anti-γ-tubulin and anti-GFP immunoblotting (WB). **(B)** The CDK5RAP2

fragments 90–140 (FLAG tagged) and 1–100 (GFP tagged) were co-expressed in HEK293T cells for anti-FLAG immunoprecipitation, and the immunoprecipitates were tested by anti-GFP and anti-FLAG immunoblotting. WT, FLAG-90–140 wild-type; S112D, FLAG-90–140(S112D). **(C)** RPE-1 stable lines of doxycycline-inducible expression of GFP-CDK5RAP2(S112D) were transfected with *cdk5rap2*-targeting or control siRNA, and the lysates were analyzed by anti-CDK5RAP2 immunoblotting. **(D)** Microtubule regrowth was performed on RPE-1 cells expressing GFP-CDK5RAP2 wild-type (WT) or S112D and depleted of endogenous CDK5RAP2 (through RNAi). Immunostaining was performed with indicated antibodies (n = 78 for centrosomal microtubule regrowth in WT- and S112D-expressing cells; n = 80 and 78 for Golgi-derived microtubule regrowth in WT- and S112D-expressing cells, respectively), and nuclei were stained with Hoechst 33258. Arrows: centrosomes; white lines: cell boundaries; white dash lines: Golgi boundaries. Box-and-whisker plots: Boxes represent the 25th and 75th percentile, "+" within boxes show averages, and whiskers mark the 10th and 90th percentile. Unpaired t test used in D; ***, P < 0.001. Scale bars, 10 µm.

After fixation, the cells were sequentially stained with primary antibodies and Alexa Fluor-conjugated secondary antibodies, and nuclear DNA was stained with Hoechst 33258 (Sigma-Aldrich). To stain γ-tubulin on the Golgi, cells were extracted with a saponin-containing buffer (0.1 M PIPES-KOH, pH 6.9, 2 M glycerol, 5 mM $MgCl_2$, 2 mM EGTA, 0.1% saponin) before methanol fixation, and the anti-γ-tubulin signal was visualized by sequential staining with two secondary antibodies (goat anti-mouse followed by donkey anti-goat) labeled with the same dye (Wang et al., 2014). Epifluorescence images were captured using a microscope (Axio Observer Z1, Carl Zeiss) equipped with an ORCA-Flash 4.0 camera (Hamamatsu Photonics) and operated using ZEN microscope software (Version 2011, Carl Zeiss). Confocal images were acquired on a Leica TCS SP8 confocal microscope equipped with supersensitive HyD detectors and using a 63× oil objective and were processed by using the LAS X (Leica Application Suite X) Software Platform and the Fiji package of ImageJ.

The subcellular position of centrosomes was determined according to a reported method (Hale et al., 2011). Briefly, the cell boundary was outlined using the Freehand tool of ImageJ software, after which the cell centroid and the size of the outlined cell area were determined by the software. The cell area was converted into a circular shape to derive the effective cell radius, r_{eff}, by the formula $r_{eff} = \sqrt{(A/\pi)}$, where A is the cell area. Distances between centrosomes and the cell centroid were expressed relative to r_{eff}. To determine distances between centrosomes and the Golgi, we outlined the Golgi area and measured the shortest distances from the centrosomes to the Golgi outline. If the centrosome was embedded in the Golgi area, the distance was considered to be 0.

Cell assays

Microtubule regrowth, Golgi reassembly, and Golgi reorientation were measured as reported (Xing et al., 2016; Shen et al., 2017). To examine microtubule regrowth, cells were first chilled on ice water for 1 h to depolymerize microtubules and then rewarmed at 37°C to allow the regrowth; the regrowth was terminated by cell fixing. To quantify regrowth, Golgi-associated microtubules were counted and the intensities of centrosome-based microtubule asters were measured; data are presented after background subtraction.

In the Golgi reassembly assays, the Golgi complexes were first disassembled by treating cells with 2.5 µg/ml nocodazole for 2 h at 37°C. After washing out the nocodazole with prechilled medium, Golgi assembly was initiated at 37°C and allowed to proceed at various times. Fluorescence images were processed using ImageJ software. Background subtraction was performed and Golgi or Golgi fragments were selected according to GM130 signals using the Freehand tool. The areas of the selected Golgi or Golgi fragments were measured using the Analyze Particles tool in the ImageJ software.

In cell polarization assays, a confluent monolayer of cells was scratched with a pipette tip to create a gap (Shen et al., 2017), and at various times after scratching, the cells were fixed for immunofluorescence microscopy. To examine centrosome and Golgi reorientation, two lines were drawn from the nucleus centroid—one perpendicular to the wound edge and the other to the centrosome or the centroid of the Golgi complex (Xing et al., 2016)—and the angle between the two lines was measured; this angle represents the degree of reorientation required to position the centrosome or the Golgi facing straight toward the wound edge.

Immunoprecipitation, pulldown, and in vitro binding assays

Cell extracts were prepared at 4°C in lysis buffer (50 mM HEPES, pH 7.4, 150 mM NaCl, 1 mM EGTA, 1 mM $MgCl_2$, 1 mM dithiothreitol, Roche Complete Protease Inhibitor Cocktail) containing 0.5% IGEPAL CA-630 (Sigma-Aldrich) and clarified by centrifugation in a microcentrifuge. The extracts were incubated with the following beads as indicated for 2 h at 4°C with rotation: anti-FLAG M2-coupled beads (Sigma-Aldrich), M-280 streptavidin beads (Invitrogen), or Protein A-agarose beads (Thermo Fisher Scientific) coupled with primary antibody. The beads were subsequently collected by centrifugation and extensively washed in lysis buffer containing 0.1% IGEPAL CA-630, and the bound proteins were eluted and analyzed through SDS-PAGE and immunoblotting. To test protein binding in vitro, recombinant proteins were incubated in lysis buffer containing 0.1% IGEPAL CA-630 and 2 mg/ml bovine serum albumin at 4°C for 2 h, and then the proteins were immunoprecipitated and immunoblotted.

Protein phosphorylation

The recombinant protein His_6-FLAG-SBP-CDK5RAP2(1–140; 1 µg) was incubated with human Nek2 protein (Abcam) in a kinase buffer (50 mM Tris-HCl, pH 7.7, 10 mM $MgCl_2$, 10 mM NaF, 1 mM dithiothreitol, 0.1 mM ATP) at 30°C for 1 h. Reactions were terminated by adding SDS-PAGE sample buffer and heating at 70°C for 10 min. The proteins were then separated by SDS-PAGE and the gels were stained by GelCode Blue (Thermo Fisher Scientific). The bands corresponding to the 1–140 protein were excised for in-gel tryptic digestion. The resulting peptides were extracted, desalted using StageTips (Thermo Fisher Scientific), and analyzed by mass spectrometry using a UHPLC system coupled to a Q Exactive Plus Hybrid Quadrupole-Orbitrap mass spectrometer (Thermo Fisher Scientific). The acquired mass spectra were analyzed using Proteome Discoverer 2.5 software (Thermo Fisher Scientific) to identify the phosphorylation site of the CDK5RAP2 protein.

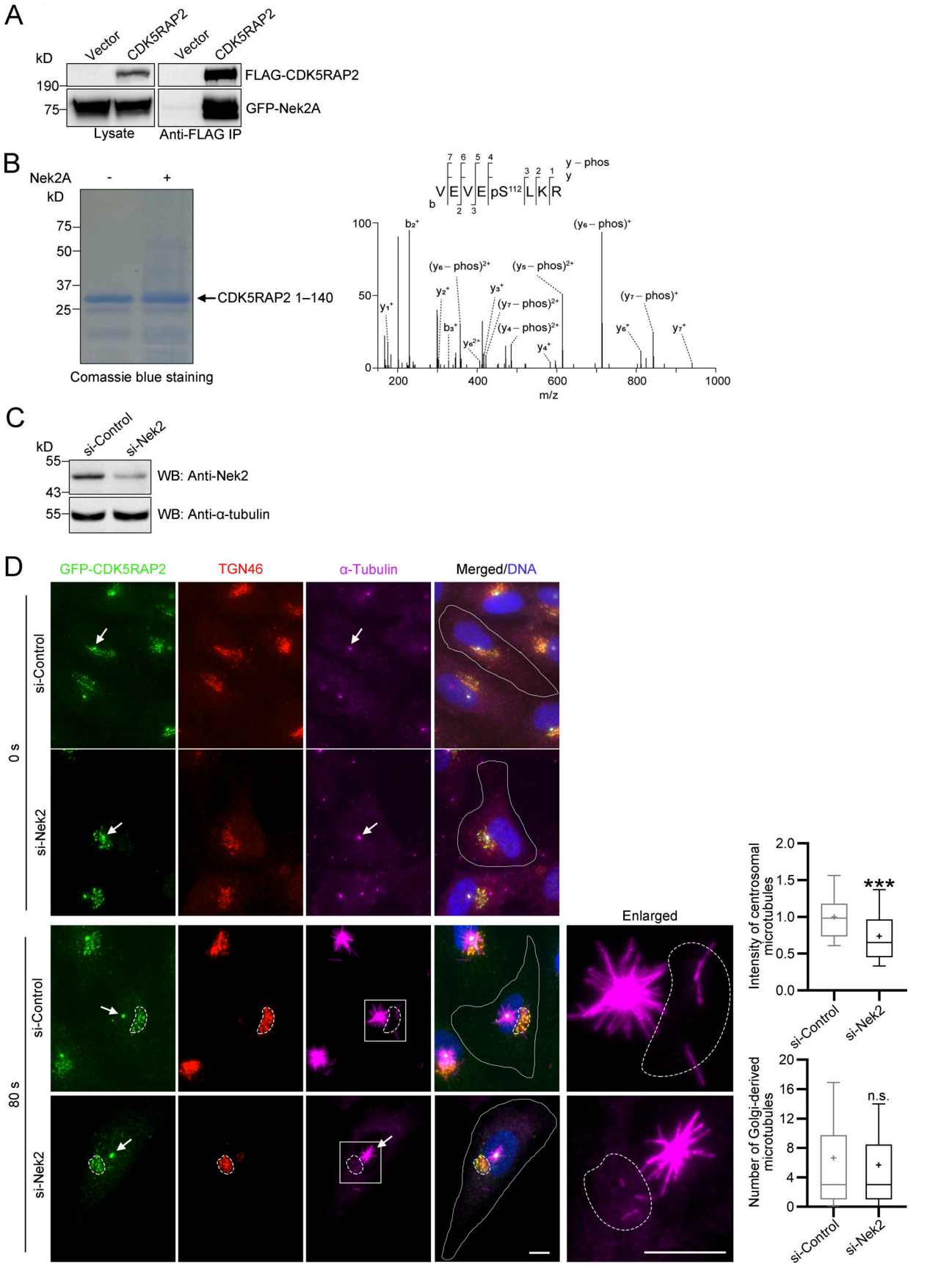

Figure 7. **Nek2 catalyzes Ser112 phosphorylation. (A)** Binding of CDK5RAP2 and Nek2A. CDK5RAP2 and Nek2A were ectopically expressed in HEK293T cells for co-immunoprecipitation. The anti-FLAG precipitates (IPs) were analyzed by immunoblotting. **(B)** Phosphorylation of the CDK5RAP2 fragment 1–140 by

Nek2A. The recombinant protein of 1–140 was subjected to an in vitro phosphorylation reaction with or without Nek2A. After the reaction, the proteins were resolved by SDS-PAGE, and the band of 1–140 was excised for mass spectrometry. Left: An SDS-PAGE gel stained with GelCode Blue. Right: A mass spectrum of the phosphoSer112-containing peptide from the Nek2A-phosphorylated sample. **(C and D)** RPE-1 cells were transfected with control or *nek2*-targeting siRNA. **(C)** The cell extracts were analyzed on antiNek2 and anti-α-tubulin immunoblots. **(D)** Microtubule regrowth was assayed on the cells after cold-induced depolymerization. Immunostaining was performed with indicated antibodies (n = 76 and 83 for centrosomal microtubule regrowth in control and Nek2-depleted cells, respectively; n = 100 and 93 for Golgi-derived microtubule regrowth in control and Nek2-depleted cells, respectively). Nuclei were stained with Hoechst 33258. Arrows: centrosomes; white lines: cell boundaries; dash lines: Golgi boundaries. Boxed areas are enlarged. Box-and-whisker plots: lower and upper edges, 25th and 75th percentiles; lower and upper whiskers, 10th and 90th percentiles; lines within boxes, medians; "+" within boxes, averages. Unpaired t test was used in D. ***, P < 0.001; n.s., not significant, P ≥ 0.05. Scale bars, 10 µm.

Statistical analysis

Statistical analyses were performed using GraphPad Prism 8 software, and all datasets were collected from at least three independent experiments. P values in experiments containing two groups were calculated using two-tailed unpaired Student's t test, P values in experiments containing multiple groups were calculated using one-way ANOVA, and P values in experiments containing two or more groups at different time points were calculated using two-way ANOVA. Data distribution was assumed to be normal, but this was not formally tested. P ≥ 0.05 was considered statistically not significant.

Online supplemental material

Fig. S1 shows microtubule nucleation of γTuRCs in the presence of γ-TuNA (1–100) or CM1 (1–126). Fig. S2 examines microtubule regrowth after nocodazole washout in cells expressing CDK5RAP2 wild-type or I104A/E105A mutant. Fig. S3 shows centrosome positions relative to the nucleus in cells expressing CDK5RAP2(I104A/E105A). Fig. S4 shows centrosome positioning in cells expressing CDK5RAP2(S112D). Fig. S5 shows the results of Golgi reassembly and cell polarization assays using S112D-expressing cells.

Data availability

The data are available from the corresponding author (qirz@ust.hk) upon any reasonable request.

Acknowledgments

This work was supported by grants from the Research Grants Council (General Research Fund 16100820 and Theme-based Research Scheme T13-605/18-W) and the Innovation and Technology Commission (ITCPD/17-9) of Hong Kong and the Shenzhen Science and Technology Committee Research Grant (SGDX20210823103200005). F.K.C. Au was supported by the Postdoctoral Fellowship Scheme (PDFS2021-6S03) of the Research Grants Council of Hong Kong.

Author contributions: R.Z. Qi and S. Yang designed the research project; S. Yang, F.K.C. Au., G. Li, and J. Lin performed the experiments; and R.Z. Qi, S. Yang, and X.D. Li wrote the manuscript.

Disclosures: The authors declare no competing interests exist.

Submitted: 16 July 2020
Revised: 3 January 2023
Accepted: 24 March 2023

References

Alfaro-Aco, R., A. Thawani, and S. Petry. 2017. Structural analysis of the role of TPX2 in branching microtubule nucleation. *J. Cell Biol.* 216:983–997. https://doi.org/10.1083/jcb.201607060

Au, F.K.C., Y. Jia, K. Jiang, I. Grigoriev, B.K.T. Hau, Y. Shen, S. Du, A. Akhmanova, and R.Z. Qi. 2017. GAS2L1 is a centriole-associated protein required for centrosome dynamics and disjunction. *Dev. Cell.* 40:81–94. https://doi.org/10.1016/j.devcel.2016.11.019

Bauer, M., F. Cubizolles, A. Schmidt, and E.A. Nigg. 2016. Quantitative analysis of human centrosome architecture by targeted proteomics and fluorescence imaging. *EMBO J.* 35:2152–2166. https://doi.org/10.15252/embj.201694462

Burakov, A., E. Nadezhdina, B. Slepchenko, and V. Rodionov. 2003. Centrosome positioning in interphase cells. *J. Cell Biol.* 162:963–969. https://doi.org/10.1083/jcb.200305082

Cervenka, I., J. Valnohova, O. Bernatik, J. Harnos, M. Radsetoulal, K. Sedova, K. Hanakova, D. Potesil, M. Sedlackova, A. Salasova, et al. 2016. Dishevelled is a NEK2 kinase substrate controlling dynamics of centrosomal linker proteins. *Proc. Natl. Acad. Sci. USA.* 113:9304–9309. https://doi.org/10.1073/pnas.1608783113

Choi, Y.-K., P. Liu, S.K. Sze, C. Dai, and R.Z. Qi. 2010. CDK5RAP2 stimulates microtubule nucleation by the γ-tubulin ring complex. *J. Cell Biol.* 191:1089–1095. https://doi.org/10.1083/jcb.201007030

Consolati, T., J. Locke, J. Roostalu, Z.A. Chen, J. Gannon, J. Asthana, W.M. Lim, F. Martino, M.A. Cvetkovic, J. Rappsilber, et al. 2020. Microtubule nucleation Properties of single human γTuRCs explained by their Cryo-EM structure. *Dev. Cell.* 53:603–617.e8. https://doi.org/10.1016/j.devcel.2020.04.019

Edelheit, O., A. Hanukoglu, and I. Hanukoglu. 2009. Simple and efficient site-directed mutagenesis using two single-primer reactions in parallel to generate mutants for protein structure-function studies. *BMC Biotechnol.* 9:61. https://doi.org/10.1186/1472-6750-9-61

Efimov, A., A. Kharitonov, N. Efimova, J. Loncarek, P.M. Miller, N. Andreyeva, P. Gleeson, N. Galjart, A.R.R. Maia, I.X. McLeod, et al. 2007. Asymmetric CLASP-dependent nucleation of noncentrosomal microtubules at the trans-Golgi network. *Dev. Cell.* 12:917–930. https://doi.org/10.1016/j.devcel.2007.04.002

Fong, K.-W., Y.-K. Choi, J.B. Rattner, and R.Z. Qi. 2008. CDK5RAP2 is a pericentriolar protein that functions in centrosomal attachment of the γ-tubulin ring complex. *Mol. Biol. Cell.* 19:115–125. https://doi.org/10.1091/mbc.e07-04-0371

Fry, A.M., P. Meraldi, and E.A. Nigg. 1998. A centrosomal function for the human Nek2 protein kinase, a member of the NIMA family of cell cycle regulators. *EMBO J.* 17:470–481. https://doi.org/10.1093/emboj/17.2.470

Hale, C.M., W.-C. Chen, S.B. Khatau, B.R. Daniels, J.S.H. Lee, and D. Wirtz. 2011. SMRT analysis of MTOC and nuclear positioning reveals the role of EB1 and LIC1 in single-cell polarization. *J. Cell Sci.* 124:4267–4285. https://doi.org/10.1242/jcs.091231

Hanafusa, H., S. Kedashiro, M. Tezuka, M. Funatsu, S. Usami, F. Toyoshima, and K. Matsumoto. 2015. PLK1-dependent activation of LRRK1 regulates spindle orientation by phosphorylating CDK5RAP2. *Nat. Cell Biol.* 17:1024–1035. https://doi.org/10.1038/ncb3204

Haren, L., M.-H. Remy, I. Bazin, I. Callebaut, M. Wright, and A. Merdes. 2006. NEDD1-dependent recruitment of the γ-tubulin ring complex to the centrosome is necessary for centriole duplication and spindle assembly. *J. Cell Biol.* 172:505–515. https://doi.org/10.1083/jcb.200510028

Hurtado, L., C. Caballero, M.P. Gavilan, J. Cardenas, M. Bornens, and R.M. Rios. 2011. Disconnecting the Golgi ribbon from the centrosome prevents directional cell migration and ciliogenesis. *J. Cell Biol.* 193:917–933. https://doi.org/10.1083/jcb.201011014

Katoh, Y., S. Nozaki, D. Hartanto, R. Miyano, and K. Nakayama. 2015. Architectures of multisubunit complexes revealed by a visible

immunoprecipitation assay using fluorescent fusion proteins. *J. Cell Sci.* 128:2351–2362. https://doi.org/10.1242/jcs.168740

Kollman, J.M., A. Merdes, L. Mourey, and D.A. Agard. 2011. Microtubule nucleation by γ-tubulin complexes. *Nat. Rev. Mol. Cell Biol.* 12:709–721. https://doi.org/10.1038/nrm3209

Kollman, J.M., A. Zelter, E.G.D. Muller, B. Fox, L.M. Rice, T.N. Davis, and D.A. Agard. 2008. The structure of the γ-tubulin small complex: Implications of its architecture and flexibility for microtubule nucleation. *Mol. Biol. Cell.* 19:207–215. https://doi.org/10.1091/mbc.e07-09-0879

Letort, G., F. Nedelec, L. Blanchoin, and M. Théry. 2016. Centrosome centering and decentering by microtubule network rearrangement. *Mol. Biol. Cell.* 27:2833–2843. https://doi.org/10.1091/mbc.E16-06-0395

Lin, T.C., A. Neuner, Y.T. Schlosser, A.N. Scharf, L. Weber, and E. Schiebel. 2014. Cell-cycle dependent phosphorylation of yeast pericentrin regulates γ-TuSC-mediated microtubule nucleation. *eLife.* 3:e02208. https://doi.org/10.7554/eLife.02208

Liu, P., E. Zupa, A. Neuner, A. Böhler, J. Loerke, D. Flemming, T. Ruppert, T. Rudack, C. Peter, C. Spahn, et al. 2020. Insights into the assembly and activation of the microtubule nucleator γ-TuRC. *Nature.* 578:467–471. https://doi.org/10.1038/s41586-019-1896-6

Lüders, J., U.K. Patel, and T. Stearns. 2006. GCP-WD is a γ-tubulin targeting factor required for centrosomal and chromatin-mediated microtubule nucleation. *Nat. Cell Biol.* 8:137–147. https://doi.org/10.1038/ncb1349

Lüders, J., and T. Stearns. 2007. Microtubule-organizing centres: A re-evaluation. *Nat. Rev. Mol. Cell Biol.* 8:161–167. https://doi.org/10.1038/nrm2100

Magdalena, J., T.H. Millard, and L.M. Machesky. 2003. Microtubule involvement in NIH 3T3 Golgi and MTOC polarity establishment. *J. Cell Sci.* 116:743–756. https://doi.org/10.1242/jcs.00288

Miller, P.M., A.W. Folkmann, A.R.R. Maia, N. Efimova, A. Efimov, and I. Kaverina. 2009. Golgi-derived CLASP-dependent microtubules control Golgi organization and polarized trafficking in motile cells. *Nat. Cell Biol.* 11:1069–1080. https://doi.org/10.1038/ncb1920

Moudjou, M., N. Bordes, M. Paintrand, and M. Bornens. 1996. gamma-Tubulin in mammalian cells: the centrosomal and the cytosolic forms. *J. Cell Sci.* 109:875–887. https://doi.org/10.1242/jcs.109.4.875

Petry, S., and R.D. Vale. 2015. Microtubule nucleation at the centrosome and beyond. *Nat. Cell Biol.* 17:1089–1093. https://doi.org/10.1038/ncb3220

Pufall, M.A., and B.J. Graves. 2002. Autoinhibitory domains: Modular effectors of cellular regulation. *Annu. Rev. Cell Dev. Biol.* 18:421–462. https://doi.org/10.1146/annurev.cellbio.18.031502.133614

Rale, M.J., B. Romer, B.P. Mahon, S.M. Travis, and S. Petry. 2022. The conserved centrosomin motif, γTuNA, forms a dimer that directly activates microtubule nucleation by the γ-tubulin ring complex (γTuRC). *Elife.* 11:e80053. https://doi.org/10.7554/eLife.80053

Rivero, S., J. Cardenas, M. Bornens, and R.M. Rios. 2009. Microtubule nucleation at the cis-side of the Golgi apparatus requires AKAP450 and GM130. *EMBO J.* 28:1016–1028. https://doi.org/10.1038/emboj.2009.47

Sawin, K.E., P.C.C. Lourenco, and H.A. Snaith. 2004. Microtubule nucleation at non-spindle pole body microtubule-organizing centers requires fission yeast centrosomin-related protein mod20p. *Curr. Biol.* 14:763–775. https://doi.org/10.1016/j.cub.2004.03.042

Shen, Y., P. Liu, T. Jiang, Y. Hu, F.K.C. Au, and R.Z. Qi. 2017. The catalytic subunit of DNA polymerase δ inhibits γTuRC activity and regulates Golgi-derived microtubules. *Nat. Commun.* 8:554. https://doi.org/10.1038/s41467-017-00694-2

Taverna, E., F. Mora-Bermúdez, P.J. Strzyz, M. Florio, J. Icha, C. Haffner, C. Norden, M. Wilsch-Bräuninger, and W.B. Huttner. 2016. Non-canonical features of the Golgi apparatus in bipolar epithelial neural stem cells. *Sci. Rep.* 6:21206. https://doi.org/10.1038/srep21206

Thawani, A., M.J. Rale, N. Coudray, G. Bhabha, H.A. Stone, J.W. Shaevitz, and S. Petry. 2020. The transition state and regulation of γ-TuRC-mediated microtubule nucleation revealed by single molecule microscopy. *Elife.* 9:e54253. https://doi.org/10.7554/eLife.54253

Tovey, C.A., C. Tsuji, A. Egerton, F. Bernard, A. Guichet, M. de la Roche, and P.T. Conduit. 2021. Autoinhibition of Cnn binding to γ-TuRCs prevents ectopic microtubule nucleation and cell division defects. *J. Cell Biol.* 220:e202010020. https://doi.org/10.1083/jcb.202010020

Vinogradova, T., R. Paul, A.D. Grimaldi, J. Loncarek, P.M. Miller, D. Yampolsky, V. Magidson, A. Khodjakov, A. Mogilner, and I. Kaverina. 2012. Concerted effort of centrosomal and Golgi-derived microtubules is required for proper Golgi complex assembly but not for maintenance. *Mol. Biol. Cell.* 23:820–833. https://doi.org/10.1091/mbc.e11-06-0550

Wang, Z., T. Wu, L. Shi, L. Zhang, W. Zheng, J.Y. Qu, R. Niu, and R.Z. Qi. 2010. Conserved motif of CDK5RAP2 mediates its localization to centrosomes and the Golgi complex. *J. Biol. Chem.* 285:22658–22665. https://doi.org/10.1074/jbc.M110.105965

Wang, Z., C. Zhang, and R.Z. Qi. 2014. A newly identified myomegalin isoform functions in Golgi microtubule organization and ER-Golgi transport. *J. Cell Sci.* 127:4904–4917. https://doi.org/10.1242/jcs.155408

Wieczorek, M., T.-L. Huang, L. Urnavicius, K.-C. Hsia, and T.M. Kapoor. 2020a. MZT proteins form multi-faceted structural modules in the γ-tubulin ring complex. *Cell Rep.* 31:107791. https://doi.org/10.1016/j.celrep.2020.107791

Wieczorek, M., L. Urnavicius, S.-C. Ti, K.R. Molloy, B.T. Chait, and T.M. Kapoor. 2020b. Asymmetric molecular architecture of the human γ-tubulin ring complex. *Cell.* 180:165–175.e16. https://doi.org/10.1016/j.cell.2019.12.007

Wu, J., and A. Akhmanova. 2017. Microtubule-organizing centers. *Annu. Rev. Cell Dev. Biol.* 33:51–75. https://doi.org/10.1146/annurev-cellbio-100616-060615

Xing, M., M.C. Peterman, R.L. Davis, K. Oegema, A.K. Shiau, and S.J. Field. 2016. GOLPH3 drives cell migration by promoting Golgi reorientation and directional trafficking to the leading edge. *Mol. Biol. Cell.* 27:3828–3840. https://doi.org/10.1091/mbc.E16-01-0005

Yadav, S., S. Puri, and A.D. Linstedt. 2009. A primary role for Golgi positioning in directed secretion, cell polarity, and wound healing. *Mol. Biol. Cell.* 20:1728–1736. https://doi.org/10.1091/mbc.e08-10-1077

Zhang, J., and T.L. Megraw. 2007. Proper recruitment of γ-tubulin and D-TACC/Msps to embryonic Drosophila centrosomes requires Centrosomin Motif 1. *Mol. Biol. Cell.* 18:4037–4049. https://doi.org/10.1091/mbc.e07-05-0474

Zhu, J., A. Burakov, V. Rodionov, and A. Mogilner. 2010. Finding the cell center by a balance of dynein and myosin pulling and microtubule pushing: A computational study. *Mol. Biol. Cell.* 21:4418–4427. https://doi.org/10.1091/mbc.e10-07-0627

Supplemental material

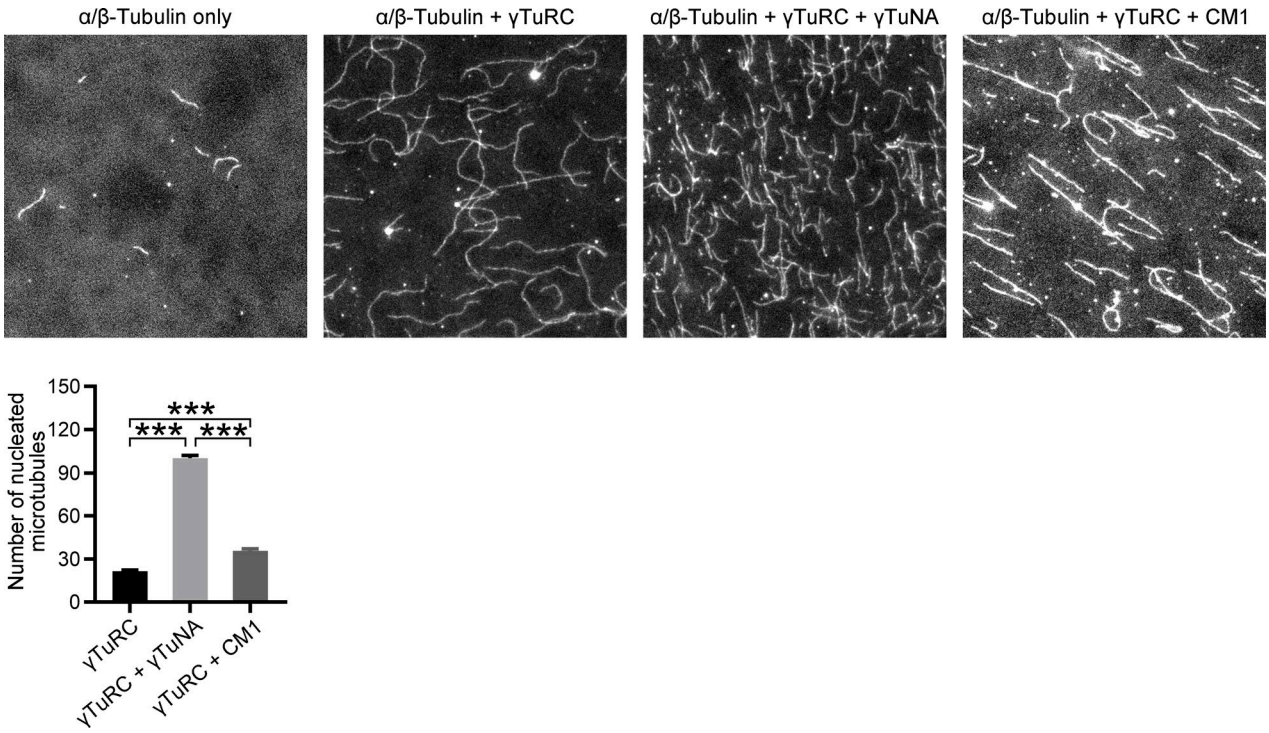

Figure S1. **Microtubule nucleation of γTuRCs stimulated by the γTuNA and CM1.** γTuRCs isolated from HEK293T cells were incubated with the recombinant proteins of γTuNA (CDK5RAP2 1–100) or CM1 (CDK5RAP2 1–126). The proteins were then added into a mixture of rhodamine-labeled and unlabeled α/β-tubulin, and microtubule polymerization was conducted at 30°C for 7 min. After terminating the reaction with a fixation buffer containing glutaraldehyde, polymerized microtubules were sedimented onto coverslips by centrifugation for fluorescence imaging. Data are presented as means ± SEM from at least three independent experiments. One-way ANOVA was used; ***, $P < 0.001$.

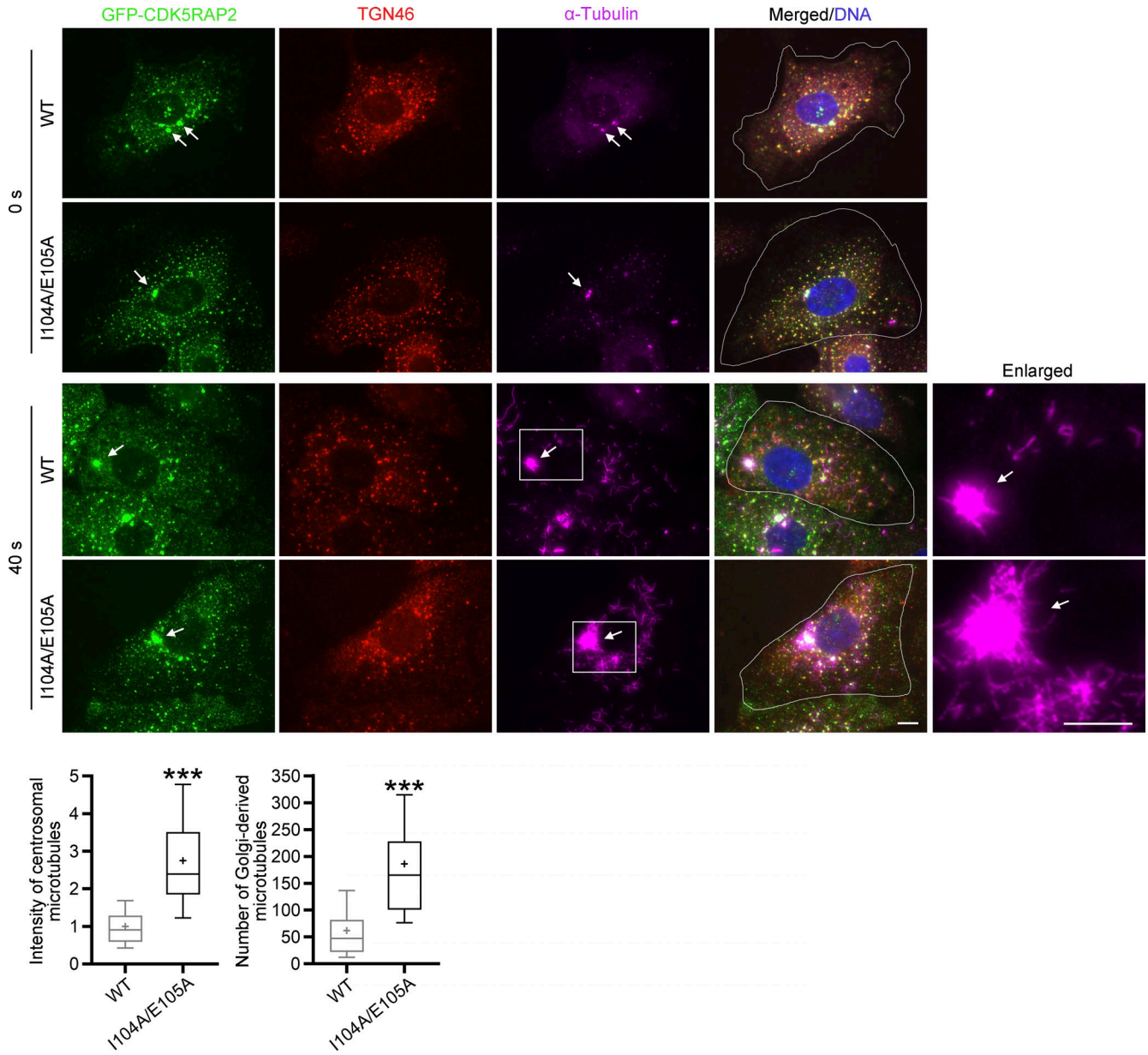

Figure S2. **Microtubule regrowth after nocodazole washout.** RPE-1 sublines expressing GFP-CDK5RAP2 wild-type (WT) or I104A/E105A mutant were depleted of endogenous CDK5RAP2 (through RNAi). The cells were treated with 2.5 µg/ml nocodazole for 2 h at 37°C, chilled on ice water for 1 h, and washed with prechilled medium. After washing, microtubule regrowth was initiated by transferring the cells to a prewarmed medium and the regrowth proceeded at 37°C for 40 s. The cells were then fixed and immunostained with indicated antibodies (n = 125 and 126 for centrosome-based regrowth in WT- and I104A/E105A-expressing cells, respectively; n = 91 and 90 for Golgi-derived regrowth in WT- and I104A/E105A-expressing cells, respectively). Nuclei were stained with Hoechst 33258. Arrows: centrosomes; white lines: cell boundaries. Boxed areas are enlarged. Box-and-whisker plot: "+" within boxes, averages. Unpaired t test was used; ***, $P < 0.001$. Scale bars, 10 µm.

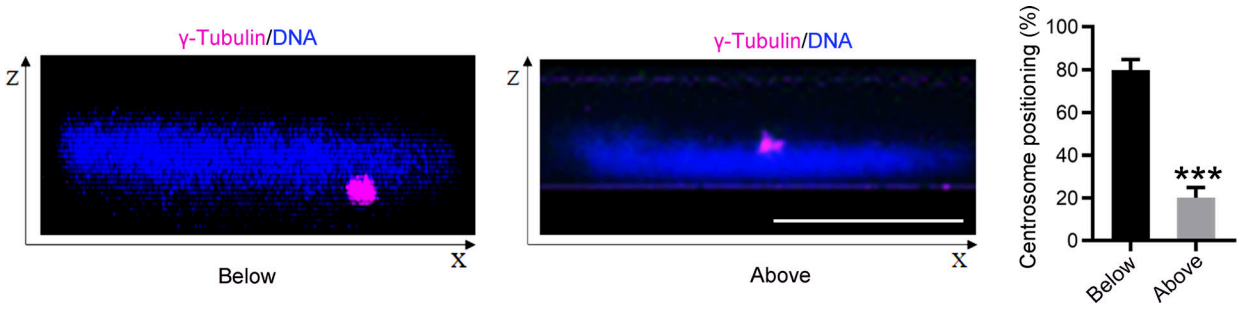

Figure S3. **Centrosome positioning relative to the nucleus in cells expressing CDK5RAP2(I104A/E105A).** RPE-1 sublines with inducible expression of GFP-CDK5RAP2(I104A/E105A) were transfected with *cdk5rap2*-targeting siRNA to deplete the endogenous protein. The cells were immunostained and imaged by 3D confocal scanning microscopy. Centrosomes located above or below the nuclei were quantified from three independent experiments (n = 46 cells). Data are presented as means ± SEM from at least three independent experiments. Unpaired *t* test used; ***, P < 0.001. Scale bar, 10 µm.

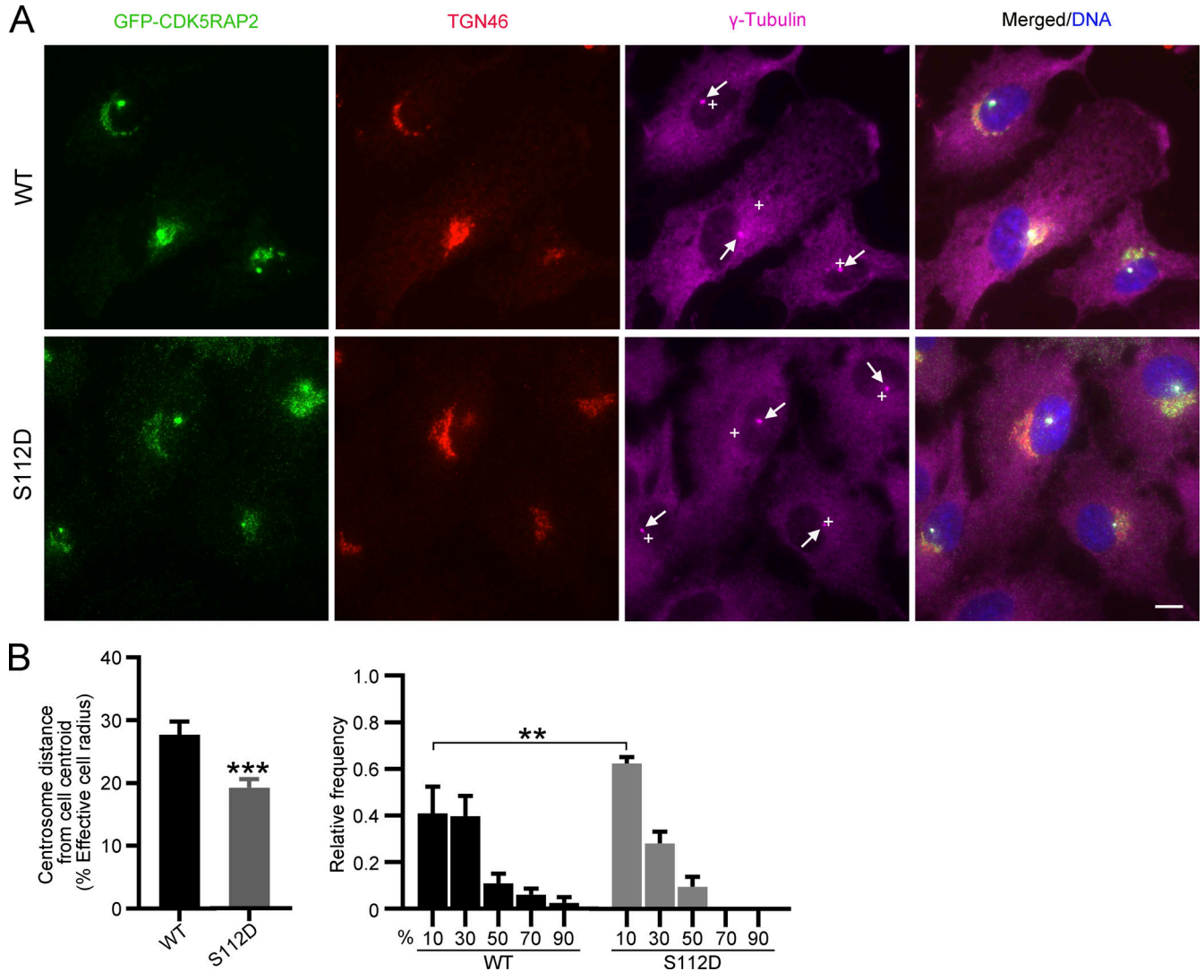

Figure S4. **Phosphomimetic mutation of Ser112 affects centrosome positioning.** RPE-1 sublines with inducible expression of GFP-tagged CDK5RAP2 wild-type (WT) and S112D mutant were subjected to RNAi-mediated depletion of endogenous CDK5RAP2. Nuclei were stained with Hoechst 33258. **(A)** Representative cell images are shown. "+", cell centroid; arrows: centrosomes. Scale bar, 10 µm. **(B)** Distances between centrosomes and cell centroids are presented as values relative to effective cell radius (left) or as frequency distributions (right). Data are presented as means ± SEM from at least three independent experiments (*n* = 83 and 85 for WT- and S112D-expressing cells, respectively). Unpaired *t* test was used in B (left) and two-way ANOVA was used in B (right); ***, P < 0.001; **, P < 0.01.

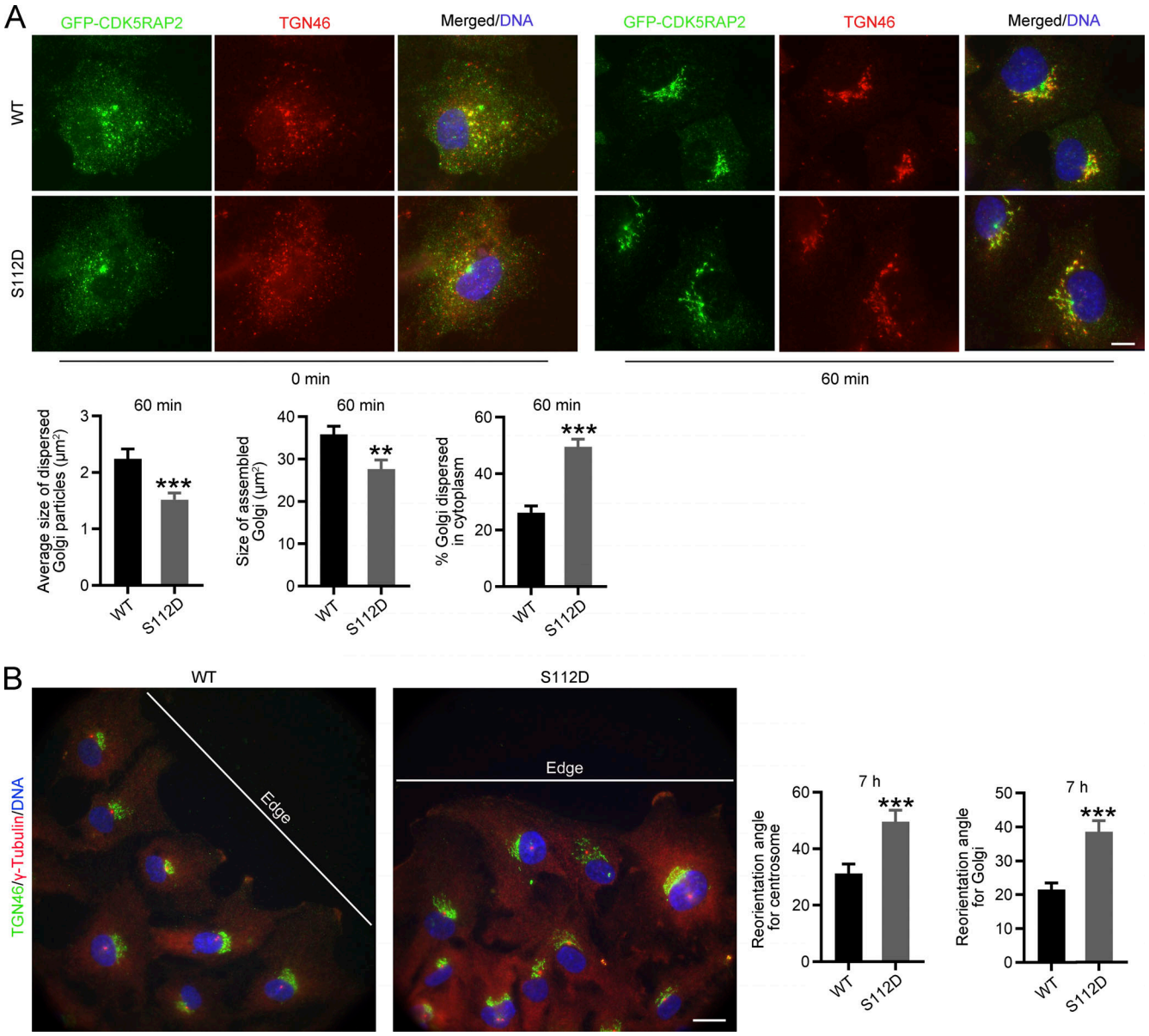

Figure S5. **Phosphomimetic mutation of Ser112 affects Golgi reassembly and cell polarization.** RPE-1 sublines were induced to express GFP-tagged CDK5RAP2 wild-type (WT) and S112D mutant, and endogenous CDK5RAP2 was depleted through RNAi. **(A)** Golgi reassembly after nocodazole washout was performed for 60 min. Cells were fixed before and after the reassembly for immunofluorescence staining; nuclear DNA was stained with Hoechst 33258. *n* = 81 for each of the WT- and S112D-expressing cells. The average size of individual Golgi particles dispersed in the cytoplasm, the size of Golgi assembled near the centrosomes, and the proportion of Golgi dispersed in the cytoplasm were determined. **(B)** Reorientation of centrosomes and Golgi was measured at 7 h after wounding. Cells were stained for TGN46, γ-tubulin, and nuclear DNA; *n* = 76 for each of WT- and S112D-expressing cells. **(A and B)** Data are presented as means ± SEM from at least three independent experiments. Unpaired *t* test used; ***, P < 0.001; **, P < 0.01. Scale bars, 10 and 20 μm in A and B, respectively.